Int. J. Electrochem. Sci., 10 **(2015)** 2716 - 2739

International Journal of
ELECTROCHEMICAL
SCIENCE
www.electrochemsci.org

Synergistic Corrosion Inhibition Effects of Coptis Extract/Berberine and Thiourea on the Corrosion of Mild Steel in Carbon Dioxide Saturated Brine Solution

Jingmao Zhao[1,2,*], *Hanbing Duan*[1], *Ruijing Jiang*[1,2]

[1] College of Material Science and Engineering, Beijing University of Chemical Technology, Beijing 100029, China
[2] Beijing Key Laboratory of Electrochemical Process and Technology for Materials, Beijing 100029, China
[*]E-mail: jingmaozhao@126.com

Received: 9 November 2014 / *Accepted:* 21 December 2014 / *Published:* 19 January 2015

The synergistic inhibition effects of the coptis extract (CP)/berberine (BB) and thiourea (TU) on the corrosion of mild steel in 3% NaCl solution saturated with CO_2 at 60 ˚C was investigated by potentiodynamic polarization curves, electrochemical impedance spectroscopy (EIS) and X-ray photoelectron spectroscopy (XPS) methods. CP and BB act as moderate inhibitors, and inhibition efficiency of the former is higher than that of the latter. The adsorption of them obeys Langmuir adsorption isotherm. The inhibition performance was significantly improved by the combined use of them with TU, and obvious synergistic corrosion inhibition effect was achieved.

Keywords: L360 mild steel; EIS; XPS; carbon dioxide corrosion; environment-friendly inhibitor.

1. INTRODUCTION

Corrosion of metal causes huge economic losses involving billions of dollars each year. In many industries, for example oil and gas exploration and production, petroleum refining and chemical manufacture, corrosion inhibition is widely employed [1]. CO_2 corrosion is one of the main corrosion existing in oil and gas industry. One of the most practical and economical methods for protecting industrial equipments from corrosion is the application of corrosion inhibitors [2].

The majority of well-known inhibitors are organic compounds containing heteroatoms such as O, N, or S, and multiple bonds, which allow an adsorption on the metal surface [3]. The effectiveness of these organic inhibitors can be ascribed to the presence of polar functional groups, which is commonly regarded as the reaction center for the occurrence of the adsorption process [4]. These

compounds can be adsorbed on metal surface and reduce the corrosion rate through blocking the active surface sites [5].

In order to avoid the hazard of most synthetic organic inhibitors to the environment [1, 4-12], researchers have made a focus on the use of naturally occurring substances which are cost-effective, non-toxic and eco-friendly inhibitors [1, 4-7, 9, 10, 12]. Due to their cheap, readily available, and renewable, plant extracts have been employed as effective inhibitors. These natural organic compounds are either synthesized or extracted from aromatic herbs, spices and medicinal plants through simple procedures with low cost and are biodegradable in nature [4, 7, 9].

In the past few years many studies about herb extracts used as corrosion inhibitors have been widely reported by several researchers. Ibrahim et al. [11] studied the corrosion inhibition of mild steel by thyme leaves extract in 2M HCl. Garai et al. [13] found that the crude methanolic extract of *Artemisia pallens* inhibit the corrosion of mild steel in 1 M HCl. Prabhu and Rao [12] investigated the performance of *Coriandrum sativum* L. seed extract in the inhibition of aluminium corrosion in 1 M phosphoric acid solution. Ostovari et al. [5] has studied the application of henna extract as corrosion inhibitor for mild steel in 1 M HCl solution. Lupine extract was studied for the corrosion inhibition of mild steel in 1 M sulphuric and 2 M hydrochloric acids by Abdel-Gaber et al. [10]. El-Etre [8] investigated khillah extract as corrosion inhibitor for SX 316 steel in HCl solution. Satapathy et al. [4] have studied the anticorrosion activity of *Justicia gendarussa* plant extract for mild steel in 1 M HCl medium. Pradeep Kumar and Mohana [1] used the extracts of *Pterolobium hexapetalum* and *Celosia argentea* plant as corrosion inhibitor for mild steel in industrial water medium. *Phyllanthus amarus* extract was investigated for its anticorrosion activity on mild steel in acidic media by Okafor et al. [9]. Bouyanzer et al. [7] studied pennyroyal oil form *Mentha pulegium* for the corrosion inhibition of steel in 1 M HCl.

Coptis chinensis is a perennial stemless herb that mainly grows in southern area of China [14]. Coptis is proven to have various biological activities such as suppression of fever, cessation of dampness, detoxification, relaxant, pyretic effects, anti-microbial, anti-fungal, anti-viral, and anti-diabetic [14-16]. Moreover, coptis is known to harbor a diversity of alkaloids, including berberine, palmatine, magnoflorine, epiberberine, and coptisine, which are considered to be its active constituents [17]. The corrosion inhibition activity of coptis extract may be ascribed to the presence of these alkaloids [9]. In particular, berberine is the most predominant component and shows various pharmacological and biological effects [14].

Li et al. [6] investigated the inhibition efficiency of berberine abstracted from *coptis chinensis* on corrosion of mild steel in 1 M H_2SO_4. Singh et al. [18] studied the inhibition of the corrosion of 7075 aluminum alloy in 3.5 wt.% NaCl solution by berberine. However, the corrosion inhibition effect of berberine on mild steel in CO_2 saturated solution has rarely been researched.

Thiourea (TU), which is presence in some commercial inhibitor formulations, is usually used in acid media [19]. As an effective corrosion inhibitor, TU has attracted lots of researchers into investigating its performance and mechanism on the corrosion of metals, owing to its strong adsorbability and its consequent influence on the interfacial characteristics [20-26]. However, it has been rarely reported about the synergistic corrosion inhibition effect between CP and TU.

This study aims to investigate the synergistic corrosion inhibition effect between CP, as well as BB, and TU on mild steel in CO_2 saturated brine solution by potentiodynamic polarization, electrochemical impedance spectroscopy (EIS) and X-ray photoelectron spectroscopy (XPS).

2. EXPERIMENTAL

2.1. Materials

Test specimens are L360 carbon steel with the following composition (wt. %): C 0.20, Si 0.45, Mn 1.60, S 0.01, P 0.02, V 0.10, Nb 0.05, Ti 0.04 and Fe balance. Specimens were machined into cylindrical samples with radius of 4 mm and thickness of 3 mm as a working electrode (WE), embedded into PVC holder using epoxy resin to make an exposed area of 0.5 cm^2, abraded with silicon carbide abrasive paper up to 1500 grit, rinsed with distilled water and degreased with acetone, then air-dried.

The aggressive solution of 3% NaCl was prepared by dilution of AR grade NaCl with distilled water. Berberine was of pure standard and obtained from Dalian Ronghai Bio-Technology Limited Company of China. The molecular structure of BB was shown in Fig. 1.

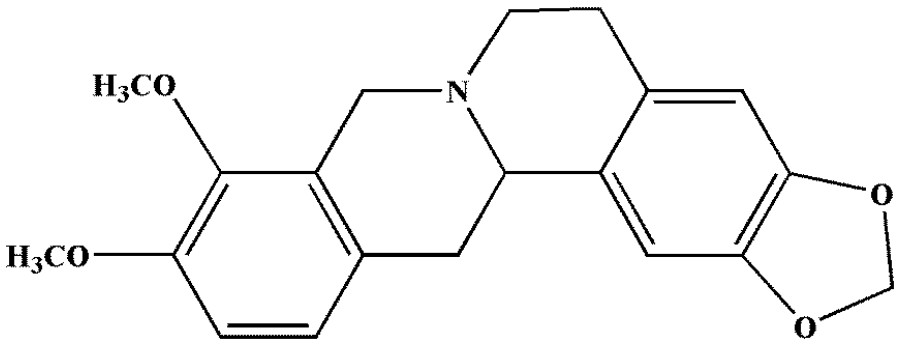

Figure 1. The molecular structures of berberine.

Coptis were bought from a Chinese medicinal herbs store in Beijing, and then dried for about 2 days in an oven at 60 ˚C, and ground to powder. Thirty gram sample of the powder was refluxed in 240 ml ethyl alcohol at 78 ˚C for 2 h by Soxhlet extractor. The above reflux process was repeated 3 times and the refluxed solution was merged. The refluxed solution was evaporated to 36 ml of dark brown residue and 36 ml 1% acetic acid solution was added into the residue. The residue was heated and filtered. In order to precipitate completely, 37% HCl solution was dropwise added into the filtered liquor. The filtered liquor was filtered again and the obtained filtered solution was dried in vacuum drying oven at 60 ˚C until complete dryness. Then the dark brown solid residue of coptis extract was obtained and preserved in conical flask.

2.2. Electrochemical measurements

A three-electrode glass cell setup with the counter electrode (CE) made of platinum and a saturated calomel electrode (SCE) as reference electrode (RE) was used during the electrochemical experiments. The CE is countered to the total exposed surface of WE. Thus, the electrical field distribution could be uniform. In order to minimize ohmic contribution, the tip of Luggin capillary was kept close to WE. The glass cell was filled with the test solution, CO_2 was bubbled through the solution for 1.5 h to remove oxygen and saturate the solution.

Electrochemical impedance spectroscopy (EIS) tests were conducted at the open circuit potential (OCP) with an ac amplitude of 10 mV in the frequency range from 100 kHz to 10 mHz. Before each test, the electrode was immersed in solutions for 30 minutes to reach a stable state (the OCP fluctuation was less than ±5 mV) [27]. The Nyquist representations of the impedance data were analyzed with Z-View software. At the end of experiment, potentiodynamic polarization was conducted over a potential range from -0.2 V to +0.2 V vs. open-circuit potential at a scan rate of 0.5 $mV \cdot s^{-1}$. Then corrosion current density (i_{corr}) and other electrochemical parameters were determined by fitting the curves in weak polarization zone using Gauss-Newton method [28, 29]. All the tests were performed at 60 ± 1 °C.

The solution and working electrode were changed after each sweep. Three to four measurements were performed for each experimental condition to estimate the repeatability, with a relative standard deviation of less than 5%.

2.3. X-ray photoelectron spectroscopy (XPS) analysis

The XPS spectra of all samples were obtained by using a PHI-5300ESCA spectrometer (Perkin–Elmer, USA) with Al Kα as excitation source. The survey scan was from 0 to 1350 eV binding energy with a step size of 1 eV. The high-resolution spectra of N 1s was acquired over 392.3 eV ~ 414.3 eV with a step size of 50 meV.

In the calibration, the binding energy of C1s was set at 284.5 eV.

The XPS spectra were deconvolved with a nonlinear least squares curve-fitting program (XPSPEAK software, Version 4.1). With a Shirley type background baseline, an asymmetrical Lorentzian–Gaussian sum function fitting program was used to process the XPS data.

3. RESULTS AND DISCUSSION

3.1 Potentiodynamic polarization

Potentiodynamic polarization curves for L360 mild steel in CO_2-saturated 3% NaCl solution with and without different concentrations of BB or CP at 60 °C are shown in Fig. 2.

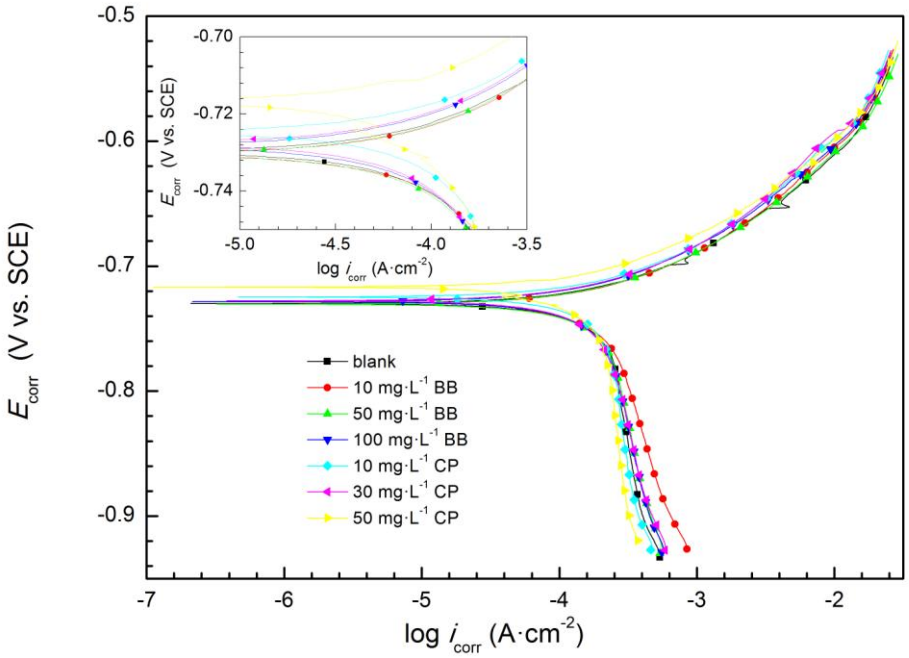

Figure 2. Potentiodynamic polarization curves for mild steel in CO_2 saturated 3% NaCl solution with and without different concentrations of BB or CP at 60 ˚C.

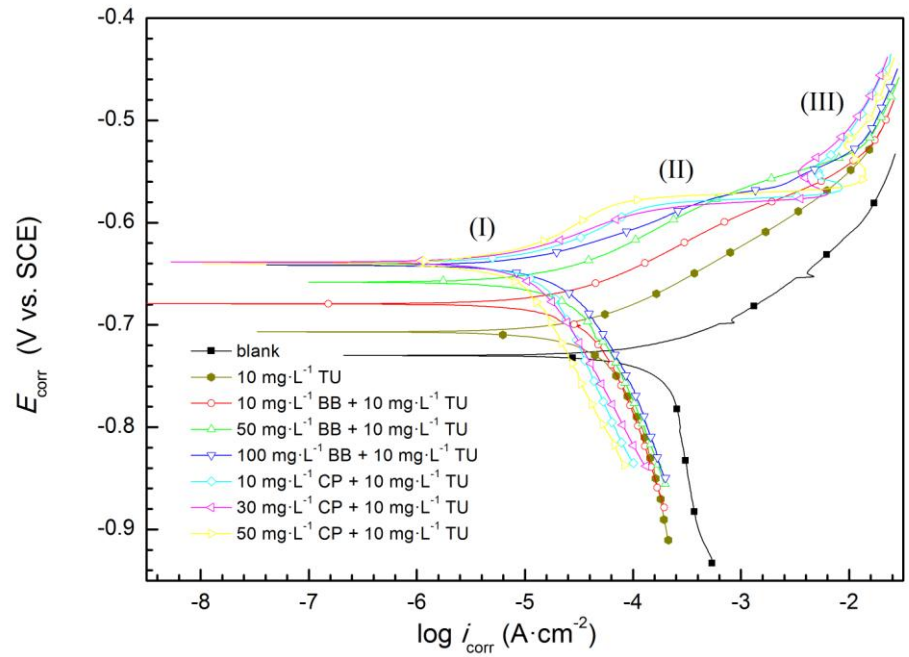

Figure 3. Potentiodynamic polarization curves for mild steel in CO_2 saturated 3% NaCl solution in the presence of 10 mg·L^{-1} TU and different concentrations of BB or CP at 60 ˚C.

From Fig. 2, it is observed that BB and CP do not improve the corrosion inhibition performance obviously. Corrosion potential (E_{corr}) does not shift remarkably and there is a small reduction in corrosion current density (i_{corr}) in the presence of individual. That is to say, both CP and BB are mixed-type inhibitors which present moderate corrosion inhibition effect. The inhibition effect of studied inhibitors increases with the increase in concentration of them. The corrosion inhibition effect of CP is better than that of BB.

Fig. 3 illustrates the potentiodynamic polarization curves for L360 mild steel in CO_2-saturated 3% NaCl solution in the presence of 10 $mg \cdot L^{-1}$ TU and different concentrations of BB or CP at 60 °C.

As seen in Fig. 3, the addition of single 10 $mg \cdot L^{-1}$ TU reduces the corrosion rates of both the cathodic hydrogen evolution and the anodic steel dissolution. When the mixtures of BB/TU or CP/TU are employed, the corrosion of mild steel is further retarded. In addition, the corrosion inhibition effect of CP/TU mixture is better than blends of BB and TU. This consequence is similar to the result that the inhibition effect of CP is superior to that of BB. As is evident from Fig. 3, a shift in both cathodic and anodic curves to lower values of corrosion current densities is observed with increase in either BB or CP concentration of inhibitor/TU mixture. In the use of BB/TU mixture, the E_{corr} gradually shifts to positive direction as BB concentration in BB/TU blends increases, which can be ascribed to that more and more cations (berberine ions) are adsorbed on the metal surface in acid solution [30]. However, this phenomenon does not arise in the CP/TU situation.

As shown in Fig. 3, three portions (I, II, and III) are observed in the anodic branch, which represent the inhibited region, flat region and uninhibited region, respectively. In portion I, the anodic currents increase moderately with the increase of anodic potentials. The commencement of portion II is a certain potential, the desorption potential (E_{des}). In this stage, the anodic currents increase steeply and a flat is observed. The flat can be attributed to the equilibrium of adsorption and desorption of inhibitor molecules on the surface of mild steel [31]. Desorption of the absorbed species on the electrode surface starts at the beginning of this region and finishes at the ending. In portion III, the anodic current densities change drastically with the potential increases. The steep increase in current is related to marked desorption of adsorbed inhibitor [32]. There is no presence of such portions in the situation and the anodic curves are similar to the curve which TU added alone, suggesting that the corrosion mechanism is not affected by the BB/TU mixture compared with the situation that TU is individually used.

The values of corrosion potential (E_{corr}), cathodic and anodic Tafel slope (β_c and β_a), and corrosion current density (i_{corr}) were deduced from the polarization curves. From the obtained i_{corr} values, the inhibition efficiency (η_p) was calculated as follows:

$$\eta_p = \left(1 - \frac{i_i}{i_u}\right) \times 100\%, \qquad (1)$$

where i_i and i_u are the inhibited and uninhibited corrosion current densities, respectively. The polarization parameters, as well as the values of η_p, are listed in Table 1.

Table 1. Electrochemical parameters and inhibition efficiency obtained from polarization measurements for mild steel in CO_2 saturated 3% NaCl solution with different concentrations of inhibitors at 60 ˚C.

BB ($mg \cdot L^{-1}$)	CP ($mg \cdot L^{-1}$)	TU ($mg \cdot L^{-1}$)	E_{corr} vs.SCE (mV)	β_a ($mV \cdot dec^{-1}$)	β_c ($mV \cdot dec^{-1}$)	i_{corr} ($\mu A \cdot cm^{-2}$)	η_p (%)
0	0	0	-728.3	55.1	-218.7	229.0	--
10	0	0	-730.4	54.2	-234.7	225.3	1.6
50	0	0	-730.4	52.5	-273.7	220.1	3. 9
100	0	0	-728.3	55.2	-218.1	192.0	16.2
0	10	0	-724.7	52.5	-272.1	220.4	3.8
0	30	0	-727.7	53.1	-257.0	204.1	10.9
0	50	0	-716.7	56.8	-195.6	177.2	22.6
0	0	10	-706.8	58.0	-183.0	46.2	79.8
10	0	10	-679.3	57.8	-185.1	32.5	85.8
50	0	10	-658.1	59.4	-170.0	27.8	87.9
100	0	10	-641.7	51.6	-301.4	24.3	89.4
0	10	10	-639.2	57.0	-193.0	17.6	92.3
0	30	10	-638.5	55.0	-220.9	13.6	94.1
0	50	10	-640.0	56.7	-197.3	9.7	95.8

From Table 1, it is demonstrated that the steel corrosion is inhibited on account of the i_{corr} value decreases when any inhibitor is added into the solution. The anodic Tafel slopes change inconspicuously compared to that of the blank solution after adding different kinds of inhibitors to solution, which suggests that the anodic corrosion process is not affected by these researched inhibitors. The cathodic corrosion process is retarded due to the increase of the cathodic Tafel slopes when BB or CP is jointly added in the solution with TU. In the presence of BB or CP alone, i_{corr} value decreases to some extent. The value of i_{corr} reduces sharply when BB/TU or CP/TU mixture is added into the solution compared with either individual inhibitor or individual TU, meaning that the steel corrosion is intensely retarded by those inhibitor blends and a strong synergistic inhibition effect is achieved between BB, as well as CP, with TU. The corrosion inhibition effect gradually becomes better when the concentration of single inhibitor increases. The highest η_p values of individual BB, CP, and TU are 16.2%, 22.6%, and 79.8% when 100 $mg \cdot L^{-1}$ BB, 50 $mg \cdot L^{-1}$ CP, and 10 $mg \cdot L^{-1}$ TU are presence, respectively. The lower η_p values of BB and CP confirms that these inhibitors have moderate inhibitive effect when used alone. It is shown in Table 1 that the η_p values follow the order: TU > CP > BB. In the presence of the mixtures of BB/TU and CP/TU, η_p values increase to corresponding 89.4% and 95.8%, indicating that these mixtures act as good inhibitors. Similarly to the situation of individual inhibitor use, the inhibition efficiency of inhibitor mixture increases with the increase in the concentration of BB or CP in the combined use with 10 $mg \cdot L^{-1}$ TU. At corresponding inhibitor concentration, η_p values follow the order: CP/TU > BB/TU.

3.2 Electrochemical impedance spectroscopy

The Nyquist plots for mild steel in 3% NaCl solutions saturated with CO2 at 60 ˚C with individual inhibitors are shown in Fig. 4.

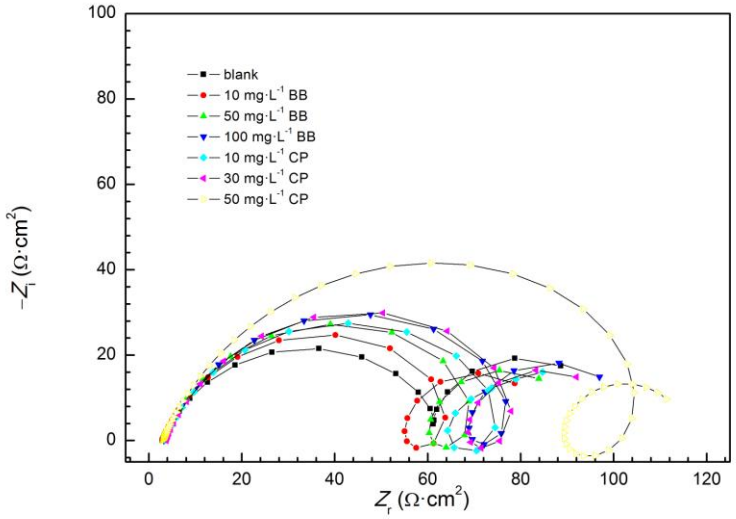

Figure 4. Nyquist plots for mild steel in CO_2 saturated 3% NaCl solution with different concentrations of BB or CP at 60 ˚C.

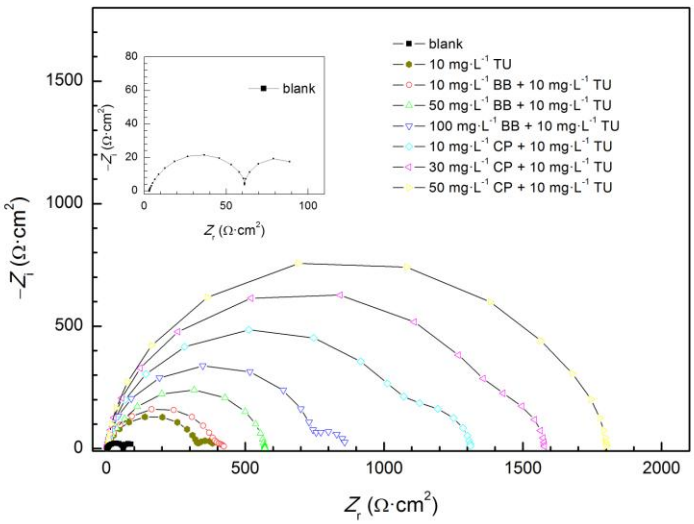

Figure 5. Nyquist plots for mild steel in CO_2 saturated 3% NaCl solution in the presence of 10 mg·L^{-1} TU and different concentrations of BB or CP at 60 ˚C.

Similar shapes of loops are observed in these plots corresponding to different concentrations of inhibitors, indicating that the corrosion mechanism does not change by adding individual BB or CP [33]. The impedance spectrum for any concentration of inhibitor is composed of a larger capacitive loop at high frequency region followed by an inductive loop and a smaller capacitive loop at low frequency region. The larger capacitive loop is related to the charge transfer resistance and the double

layer capacitance of the corrosion process at the corroding surface [34]. The inductive loop may be ascribed to the relaxation process obtained by adsorption species such as inhibitor molecules [35] or H^+_{ads} [36] on the steel surface. The smaller capacitive loop can be attributed to corrosion product resistance (R_{cp}) or inhibitor film resistance (R_f). As shown in Fig. 4, an increase in the semicircle's diameter is observed after adding inhibitor in the solution compared with that in the blank solution and the diameter increases with the inhibitor concentration increases, indicating that the addition of BB or CP can both slow the corrosion process of mild steel.

Fig. 5 shows the Nyquist plots for mild steel in 3% NaCl solutions saturated with CO_2 at 60 °C in the presence of 10 $mg \cdot L^{-1}$ TU and different concentrations of BB or CP.

As seen in Fig. 5, when the mixtures of BB/TU and CP/TU is added in the solution, the diameters of semicircles become larger than those in Fig. 4 and that of in the presence of single 10 $mg \cdot L^{-1}$ TU, suggesting that the corrosion process is further inhibited when BB or CP is jointly used with TU compared with the individual inhibitor. The diameters increase with the increase in the concentration of BB or CP in the mixtures, which is similar to the phenomenon observed in the situation when individual inhibitor is used. Noticeably, the inductive loop is disappeared after TU is added into the corroding electrolyte containing different concentrations of BB or CP. This indicates that the relaxation process is no longer presence and the corrosion process is completely under charge transfer control. From the Nyquist plots, two capacitive loops are observed, indicating that an equivalent circuit consisting of two parallel RC circuits should be used to fit the EIS results.

The depressed semicircle with a center under the real axis at high frequency range in all the Nyquist diagrams can be attributed to the roughness and other inhomogeneities of the solid electrode [37, 38].

Fig. 6a shows the electrical equivalent circuits which used to model the EIS diagrams of mild steel immersed in the solution with and without different concentrations of BB or CP. The equivalent circuits without the inductive element is used to fit EIS results obtained in the solution containing inhibitor mixtures, as well as TU, and is illustrated in Fig. 6b.

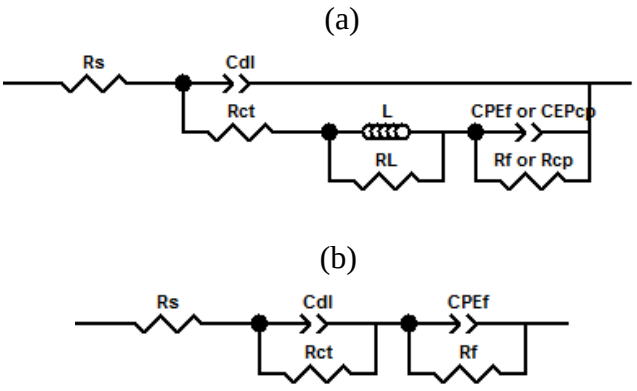

Figure 6. The equivalent circuit used to fit the impedance spectra of (a) blank, BB, and CP, (b) TU and inhibitor mixtures.

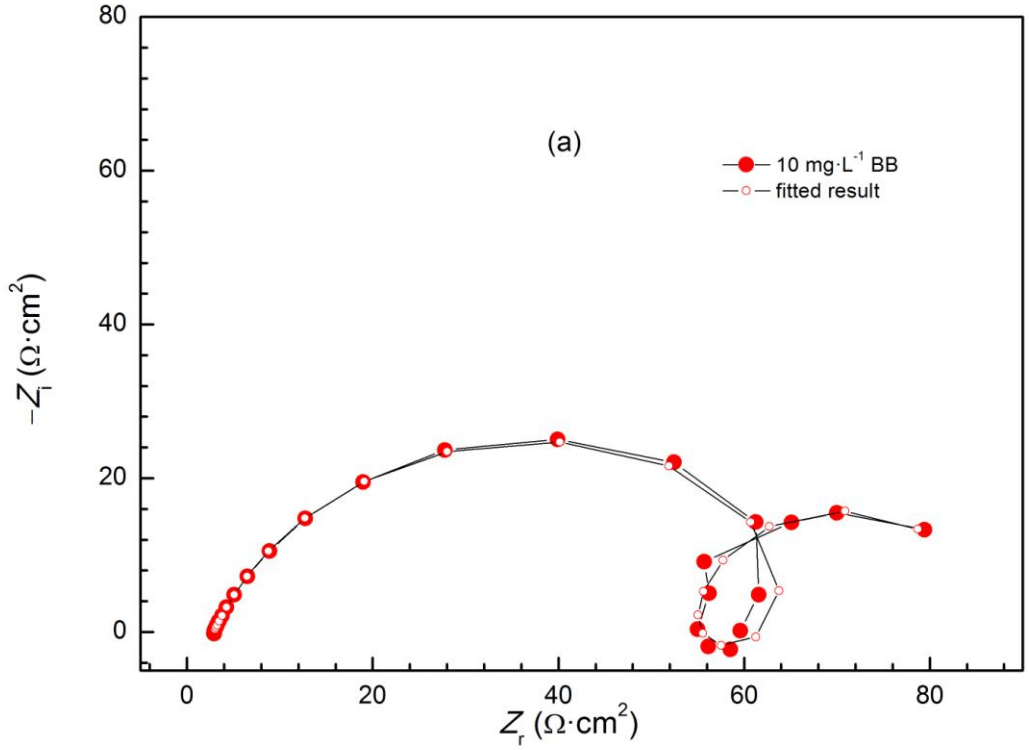
(a)
10 mg·L-1 BB
fitted result
-Zi (Ω·cm2)
Zr (Ω·cm2)
0
20
40
60
80

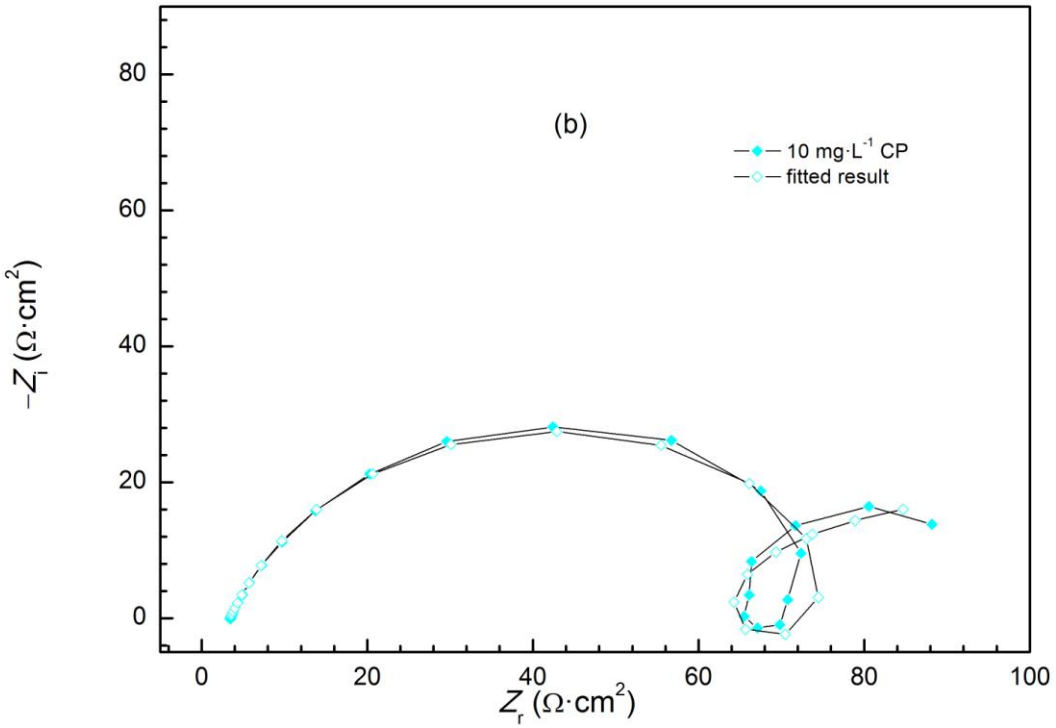
(b)
10 mg·L-1 CP
fitted result
-Zi (Ω·cm2)
Zr (Ω·cm2)
0
20
40
60
80
100

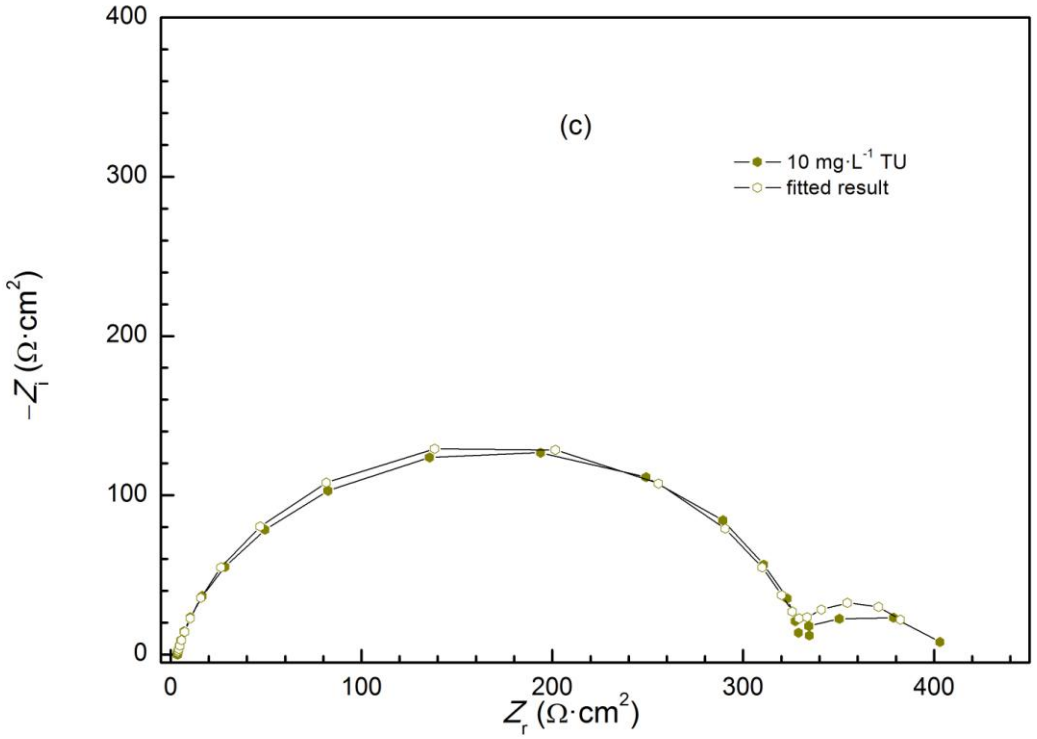
(c)
10 mg·L-1 TU
fitted result
-Zi (Ω·cm2)
Zr (Ω·cm2)
0
100
200
300
400

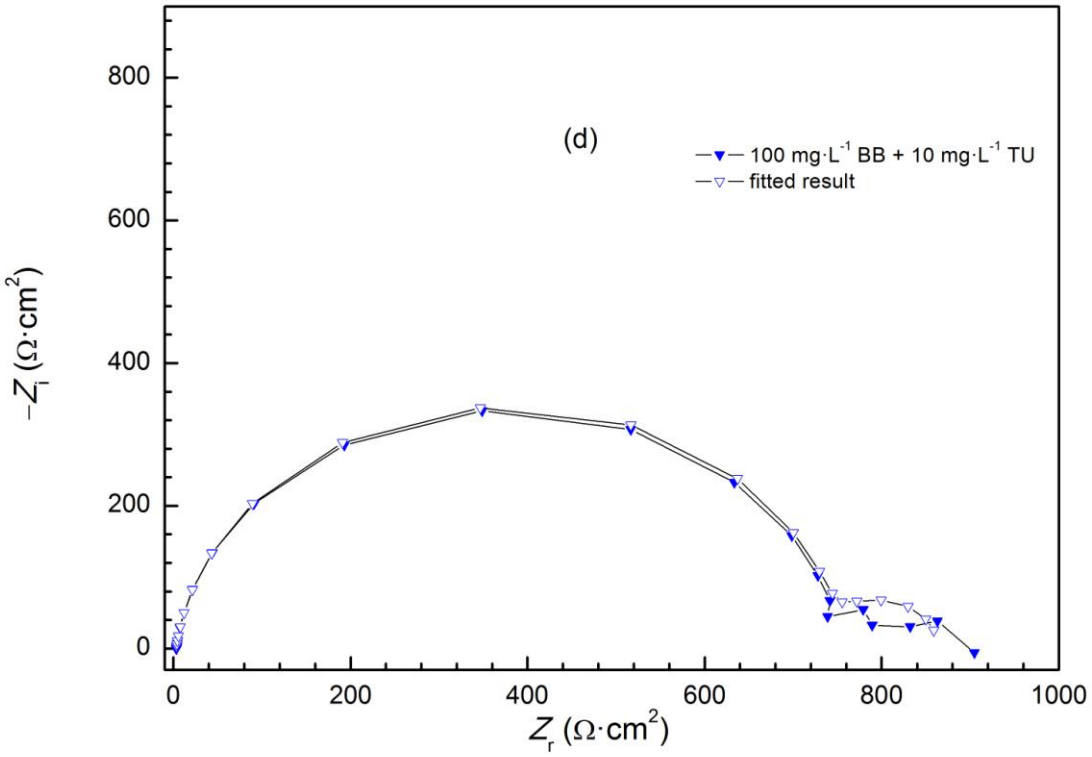
(d)
100 mg·L-1 BB + 10 mg·L-1 TU
fitted result
-Zi (Ω·cm2)
Zr (Ω·cm2)
0
200
400
600
800
1000

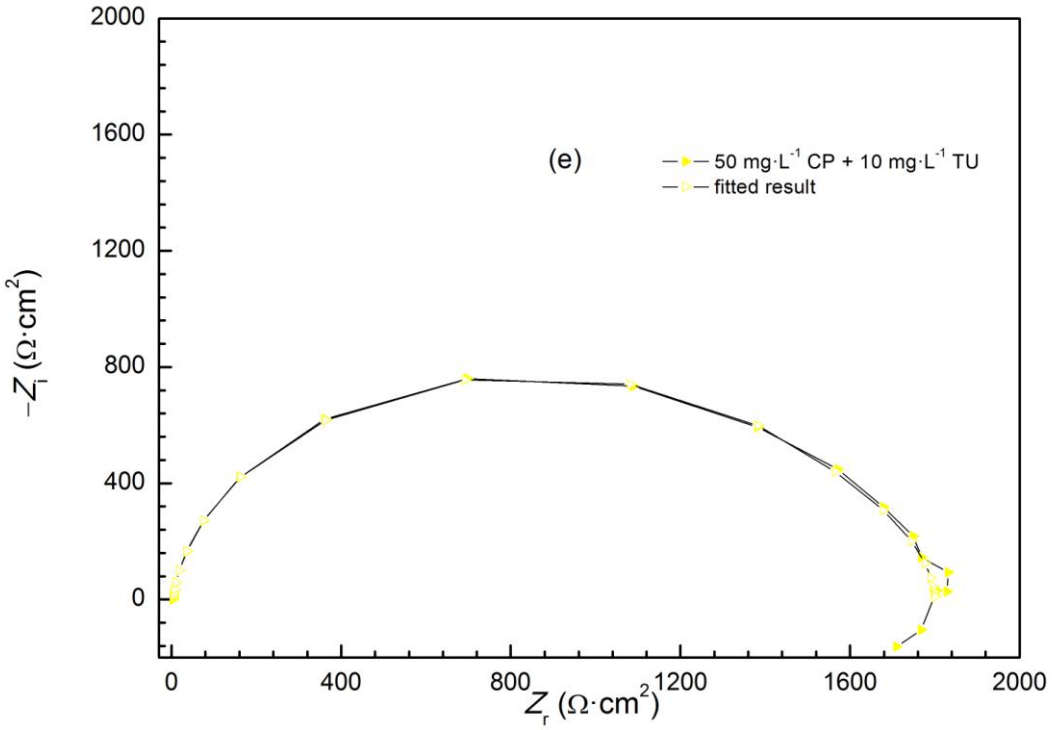

Figure 7. The representative figures of using the equivalent circuits to fit the experimental data for (a) 10 mg·L^{-1} BB, (b) 10 mg·L^{-1} CP, (c) 10 mg·L^{-1} TU, (d) 100 mg·L^{-1} BB + 10 mg·L^{-1} TU, and (e) 50 mg·L^{-1} CP + 10 mg·L^{-1} TU.

Table 2. Electrochemical impedance parameters and inhibition efficiency (η_i) obtained from EIS measurements for mild steel in CO_2 saturated 3% NaCl solution with different concentrations of inhibitors at 60 ˚C.

BB (mg·L^{-1})	CP (mg·L^{-1})	TU (mg·L^{-1})	R_s (Ω·cm^2)	CPE_{dl} (μF·cm^{-2})		C_{dl} (μF·cm^{-2})	R_{ct} (Ω·cm^2)	L (H·cm^2)	R_L (Ω·cm^2)	CPE_f (μF·cm^{-2})		R_f (or R_{cp}) (Ω·cm^2)	R_t (Ω·cm^2)	η_i (%)
				Y (s^n·cm^{-2}·Ω^{-1})	n					Y (s^n·cm^{-2}·Ω^{-1})	n			
0	0	0	3.0	7.22×10^{-4}	0.77	280.2	58.2	1.7	4.5	0.24	0.8	39.3	102.0	--
10	0	0	2.9	6.61×10^{-4}	0.78	256.2	52.5	3.0	20.1	0.28	1	31.3	103.9	1.8
50	0	0	3.1	6.63×10^{-4}	0.79	277.4	56.9	3.8	20.3	0.29	1	32.7	109.9	7.2
100	0	0	3.2	5.40×10^{-4}	0.78	210.3	65.4	3.7	19.7	0.22	1	36.2	121.3	15.9
0	10	0	3.5	6.31×10^{-4}	0.77	239.3	61.7	4.0	19.5	0.03	1	32.0	113.2	9.9
0	30	0	3.7	5.05×10^{-4}	0.78	192.5	64.9	3.4	21.5	0.30	1	32.9	119.3	14.5
0	50	0	3.0	4.12×10^{-4}	0.77	149.9	82.3	4.8	36.7	0.25	1	26.4	145.4	29.8
0	0	10	3.6	1.32×10^{-4}	0.86	75.7	328.9	--	--	0.11	1	58.3	387.2	73.7
10	0	10	3.7	1.02×10^{-4}	0.89	68.7	401.1	--	--	0.53	0.77	59.6	460.7	77.9
50	0	10	3.1	8.00×10^{-5}	0.92	60.9	539.8	--	--	1.31×10^{-4}	0.8	27.7	567.5	82.0
100	0	10	3.4	6.39×10^{-5}	0.93	50.9	752.1	--	--	3.12×10^{-3}	1	108.5	860.6	88.1
0	10	10	3.4	2.65×10^{-5}	0.92	19.5	1093	--	--	2.41×10^{-3}	0.96	216.0	1309	92.2
0	30	10	3.5	2.43×10^{-5}	0.94	19.6	1404	--	--	2.36×10^{-4}	1	171.8	1576	93.5
0	50	10	3.2	3.12×10^{-5}	0.94	25.8	1640	--	--	1.76×10^{-3}	1	157.7	1798	94.3

The representative examples of using the equivalent circuits to fit the experimental data for the solution containing 10 mg·L^{-1} BB, 10 mg·L^{-1} CP, 10 mg·L^{-1} TU, 100 mg·L^{-1} BB + 10 mg·L^{-1} TU, and 50 mg·L^{-1} CP + 10 mg·L^{-1} TU are shown in Fig. 7, respectively.

The calculated impedance parameters of interest are listed in Table 2.

As shown in Fig. 6, R_s, R_L, R_f, R_{cp}, and R_{ct} are the solution resistance, inductive resistance, inhibitor film resistance, the resistance of corrosion product, and the charge transfer resistance, respectively. L is the inductance, which is intimately associated with the inductive loop. In case of present of a non-ideal frequency response, it is commonly accepted to employ distributed circuit elements in an equivalent circuit. The constant phase element (CPE) [39] is the most widely used element, which is introduced into the circuit instead of a pure double layer capacitor (C_{dl}) in order to give a more accurate fit [40]. The CPE element is described as follow [41]:

$$Z_{CPE} = [Y(j\omega)^n]^{-1}, \quad (2)$$

where Y is the CPE constant proportional to the C_{dl} of the system, j is the imaginary number (j^2=-1), ω is the angular frequency, and n is the coefficient which reflects the extent of phase shift. The value of n determines what electrical elements the CPE represents. When n = 1 and n < 1, CPE is an ideal capacitor and a non-ideal capacitor, respectively.

R_t, which represents the total resistance of the system, is used to calculate the inhibition efficiency [41]. In individual situation and combined situation, R_t is the sum of R_L, R_f, and R_{ct}, and the sum of R_f and R_{ct}, respectively. From the calculated R_t, the inhibition efficiency (η_i) is defined as follows:

$$\eta_i = \left(1 - \frac{R_u}{R_i}\right) \times 100\% \quad (3)$$

where R_i and R_u are the inhibited and uninhibited total resistance of the system, respectively. The values of η_i are also listed in Table 2.

The R_s values which are very small suggest that the IR drop could be small. It is observed from Table 2 that adding any inhibitor into the solution causes an increase in R_t and a decrease in C_{dl}. The highest η_p values of individual BB, CP, and TU are 15.9%, 29.8%, and 73.7% when 100 mg·L^{-1} BB, 50 mg·L^{-1} CP, and 10 mg·L^{-1} TU are presence, respectively. This indicates that BB or CP can moderately retard the corrosion process in corroding system. The noteworthy result that the value of R_t increases and that of C_{dl} decreases when inhibitor mixtures are employed, respectively, confirms that there is a synergistic inhibition effect between BB/CP and TU. The corresponding η_i values are 88.1% and 94.3% for the combined use of 100 mg·L^{-1} BB + 10 mg·L^{-1} TU and that of 50 mg·L^{-1} CP + 10 mg·L^{-1} TU, respectively. It is also observed that the value of η_i increases as the concentration of individual BB or CP increases and with the increase in concentration of each inhibitor in the combined use with TU. This result is in good agreement with that obtained from potentiodynamic polarization curves. η_i follows the order: TU > CP > BB; CP/TU > BB/TU.

3.3 XPS analysis

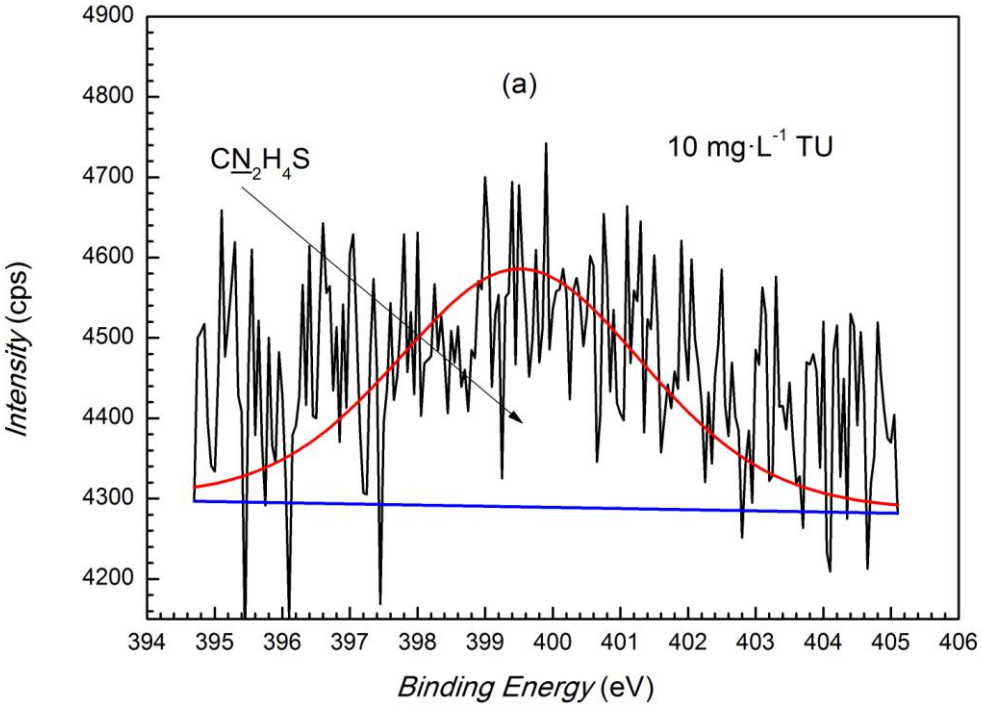

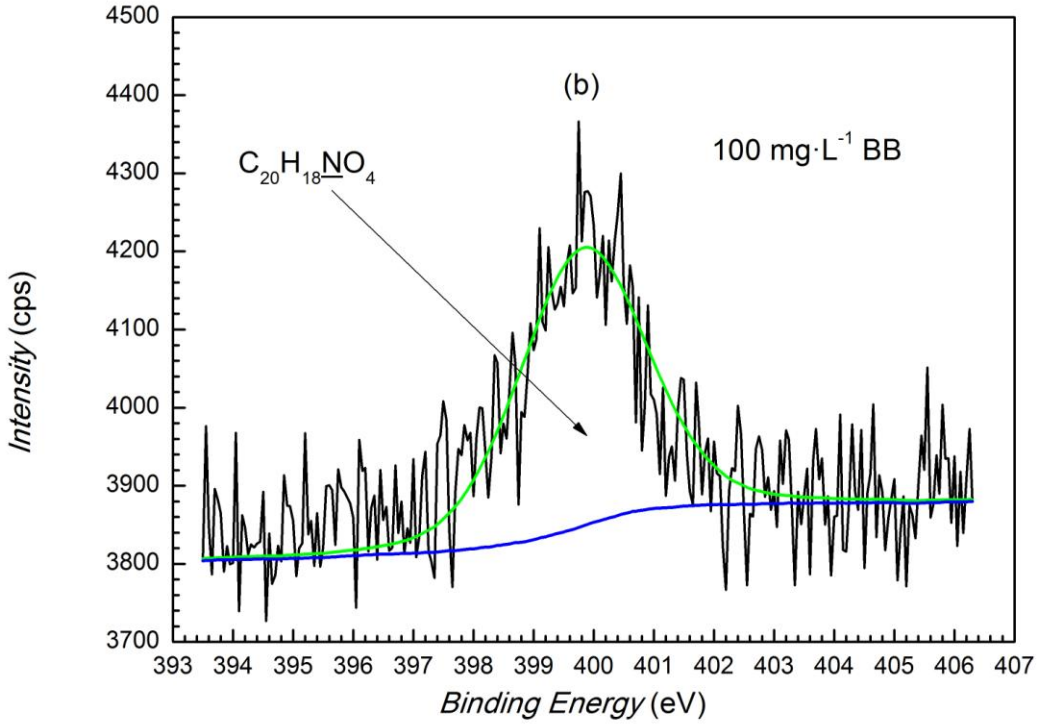

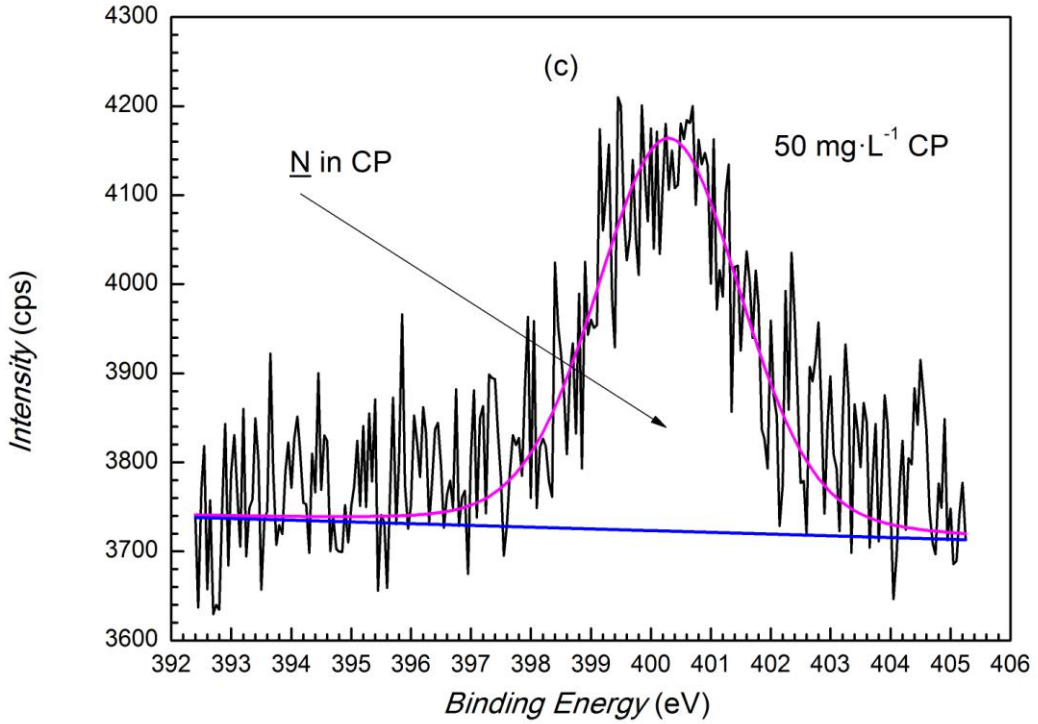
(c)
N in CP
50 mg·L-1 CP
Intensity (cps)
Binding Energy (eV)
4300
4200
4100
4000
3900
3800
3700
3600
392 393 394 395 396 397 398 399 400 401 402 403 404 405 406

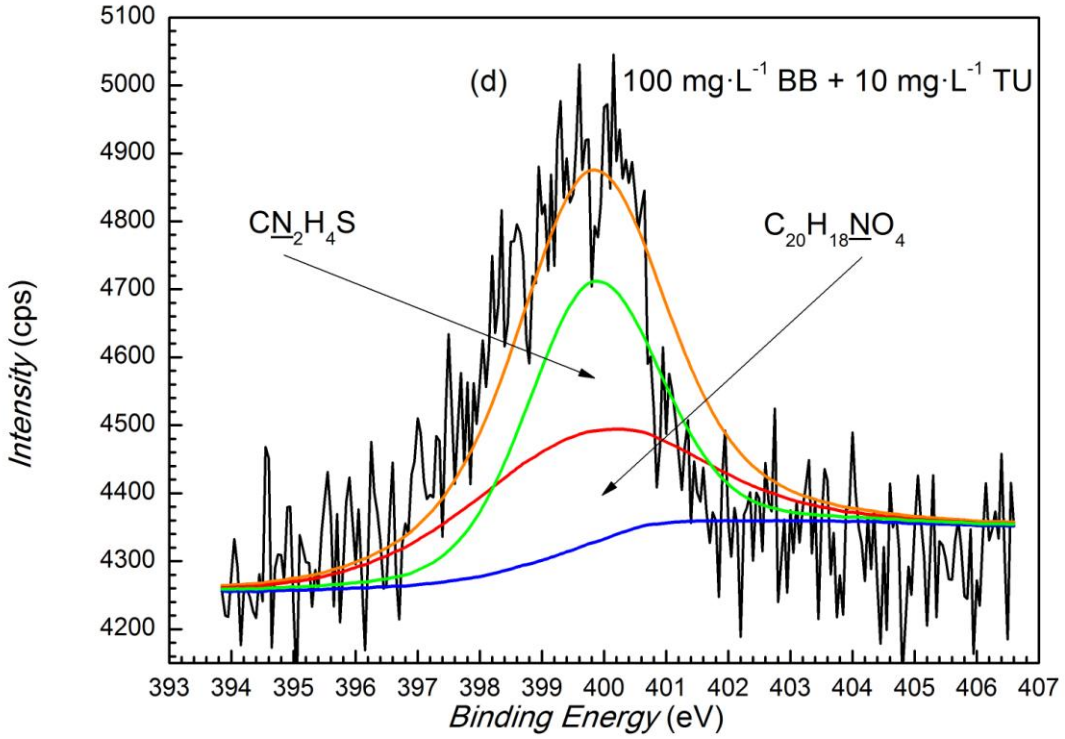
(d)
100 mg·L-1 BB + 10 mg·L-1 TU
CN2H4S
C20H18NO4
Intensity (cps)
Binding Energy (eV)
5100
5000
4900
4800
4700
4600
4500
4400
4300
4200
393 394 395 396 397 398 399 400 401 402 403 404 405 406 407

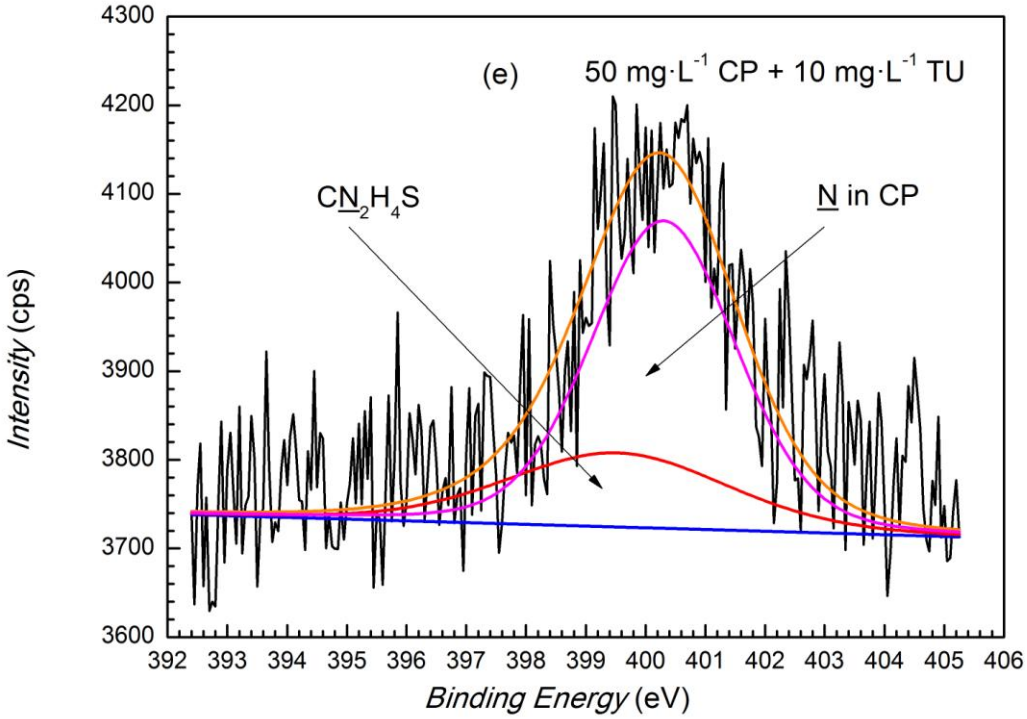

Figure 8. High-resolution XPS spectra of N 1s of mild steel obtained after immersion in CO_2 saturated 3% NaCl solution with (a) 10 mg·L^{-1} of TU, (b) 100 mg·L^{-1} of BB, (c) 50 mg·L^{-1} of CP, (d) 100 mg·L^{-1} of BB + 10 mg·L^{-1} of TU, (e) 50 mg·L^{-1} of CP + 10 mg·L^{-1} of TU at 60 ˚C.

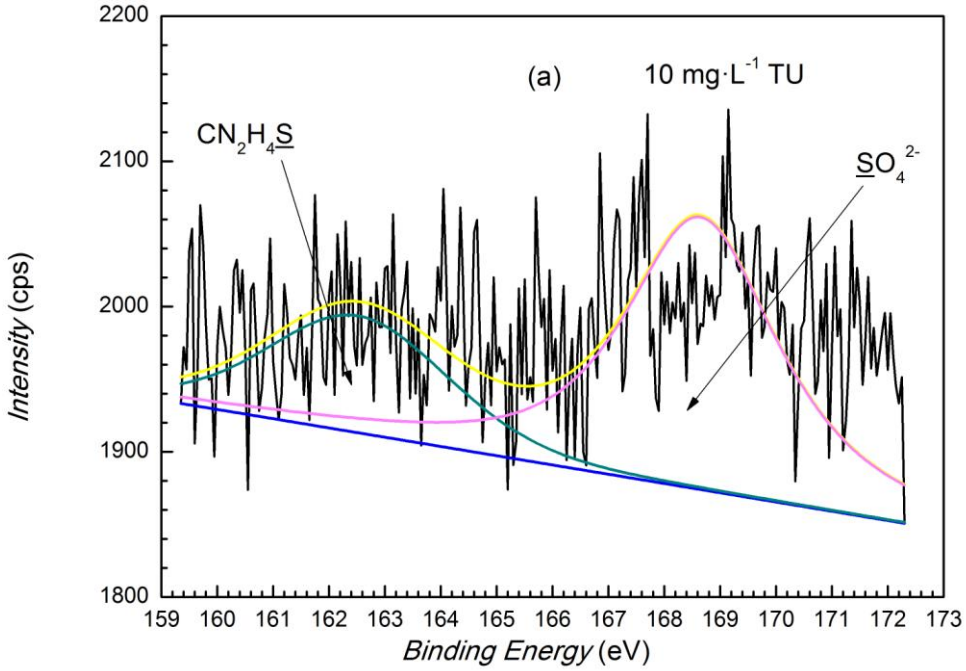

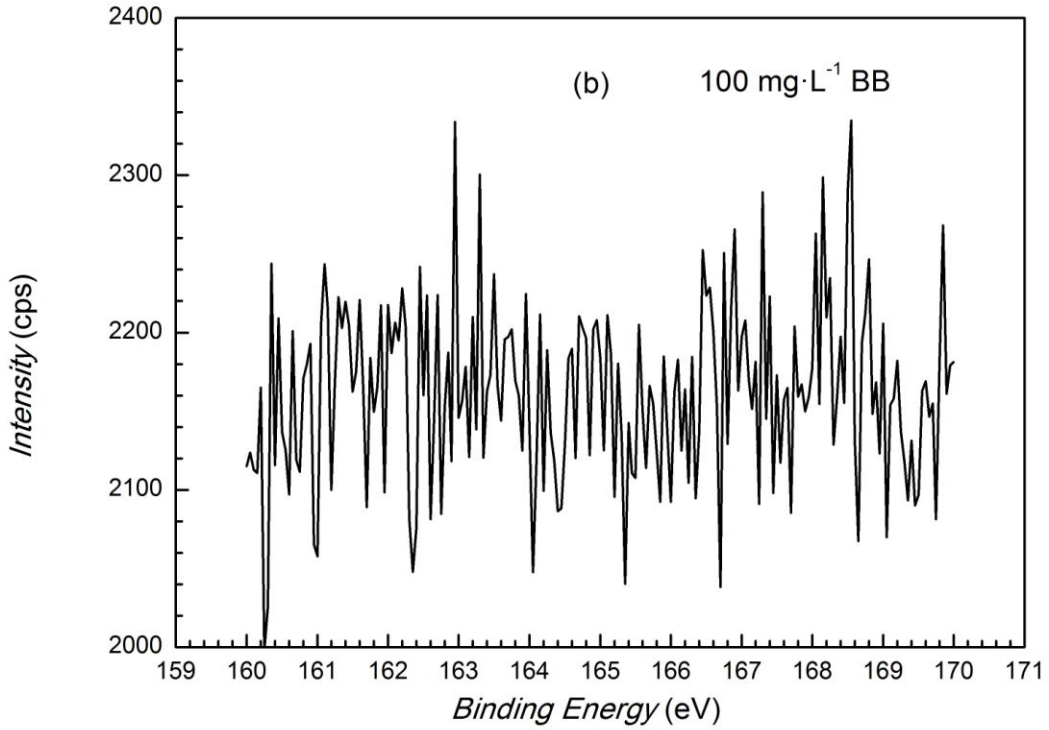
(b)
100 mg·L-1 BB
Intensity (cps)
Binding Energy (eV)
2400
2300
2200
2100
2000
159
160
161
162
163
164
165
166
167
168
169
170
171

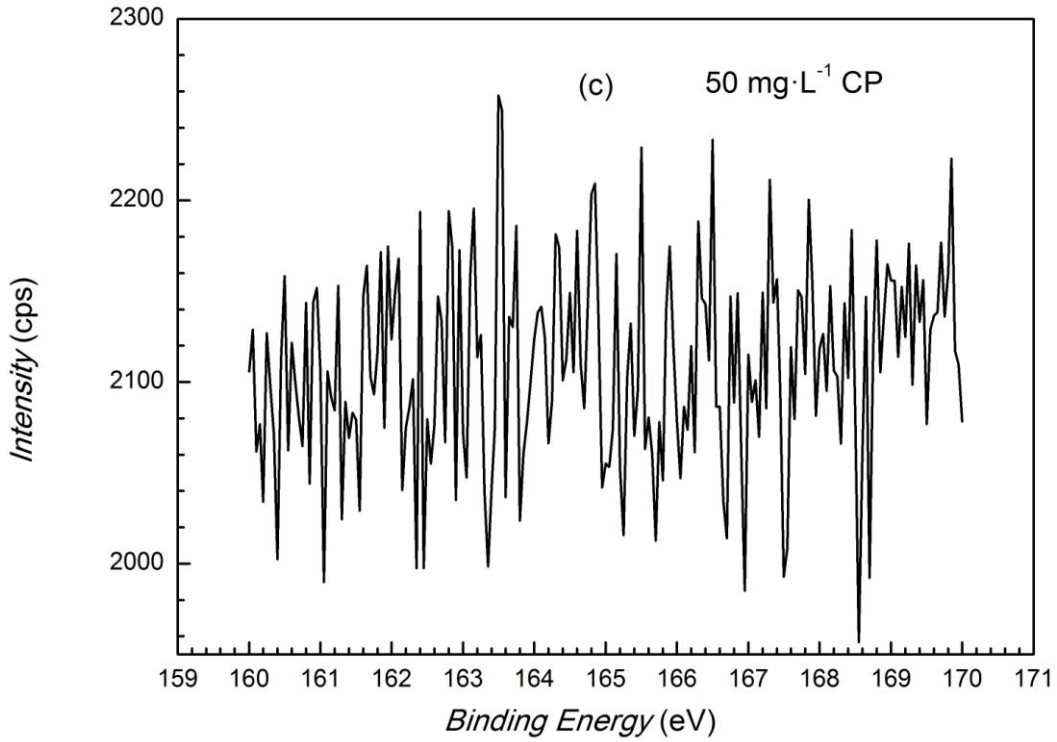
(c)
50 mg·L-1 CP
Intensity (cps)
Binding Energy (eV)
2300
2200
2100
2000
159
160
161
162
163
164
165
166
167
168
169
170
171

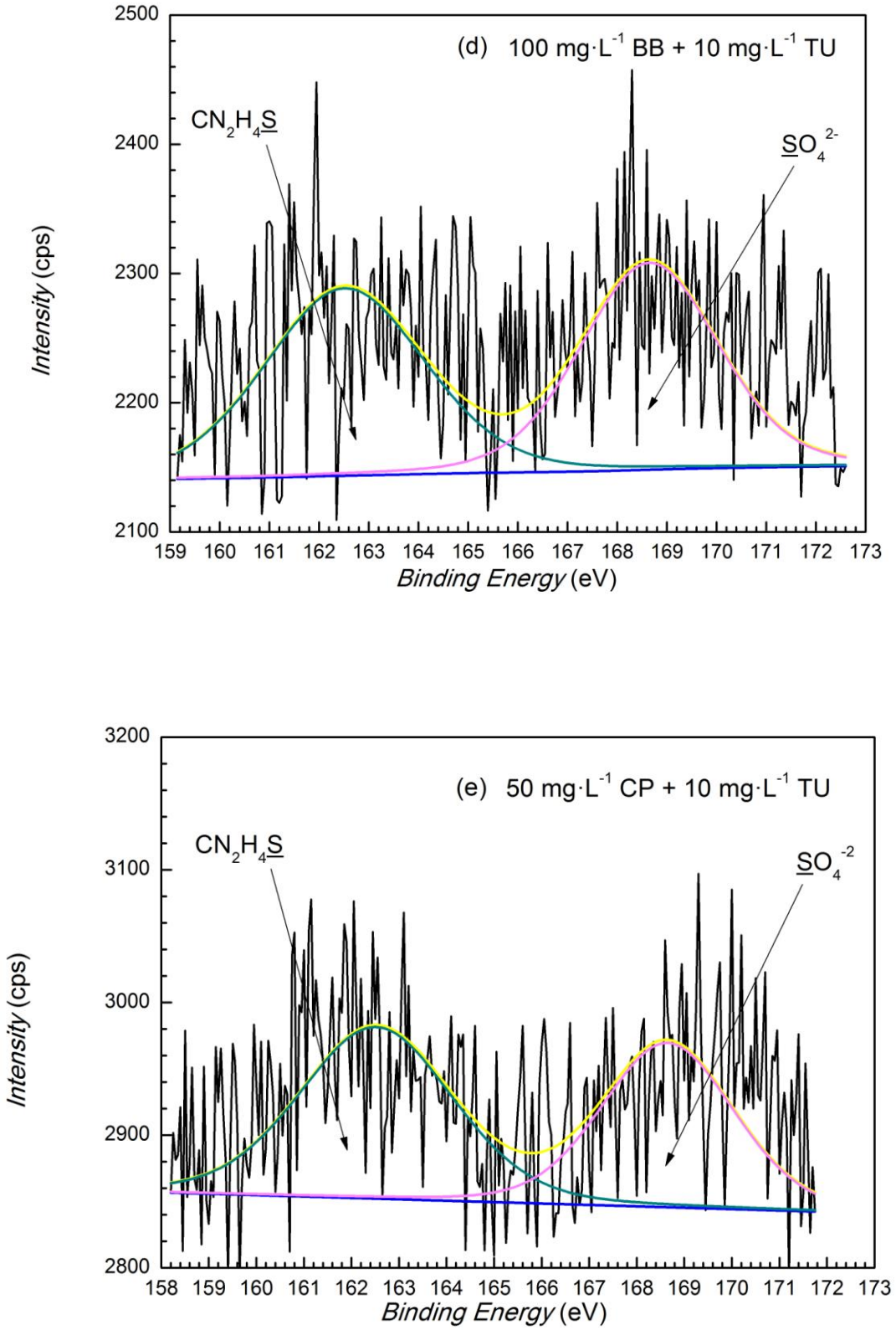

Figure 9. High-resolution XPS spectra of S 2p of mild steel obtained after immersion in CO_2 saturated 3% NaCl solution with (a) 10 mg·L^{-1} of TU, (b) 100 mg·L^{-1} of BB, (c) 50 mg·L^{-1} of CP, (d) 100 mg·L^{-1} of BB + 10 mg·L^{-1} of TU, (e) 50 mg·L^{-1} of CP + 10 mg·L^{-1} of TU at 60 ˚C.

XPS measurements of mild steel surface having been immersed in corroding solution were performed in order to investigate the adsorption behavior of inhibitors in different applications. The mild steel was immersed into the solutions with different concentrations of inhibitors for 24 hours to prepare the adsorption film and the solution should be earlier bubbled with carbon dioxide as mentioned in Section 2.2. After immersion, the samples were dried with cold air.

Figs. 8 and 9 illustrate the high-resolution XPS spectra of N 1s and S 2p of mild steel after immersion in the solution with different concentrations of inhibitors, respectively.

As shown in Fig. 8a, the N 1s peak of steel immersed in the solution containing 10 $mg \cdot L^{-1}$ TU is located at around 399.5 eV [42], which is related to nitrogen element in thiourea. Figs. 8b and 8c present the high-resolution N 1s spectra with a binging energy at 399.8 eV for 100 $mg \cdot L^{-1}$ BB and a binging energy at 400.3 eV for 50 $mg \cdot L^{-1}$ CP, respectively. The N 1s peak in Fig. 8b can be ascribed to the nitrogen element in berberine. Because of berberine is the main component of coptis, the presence of N in the XPS spectrum for mild steel immersed in the solution with CP is reasonable. However, the other components in CP may also contain N element. This could be the reason why the N 1s peak position of BB and CP is different. Figs. 8d and 8e show the N 1s line deconvolution curves for 100 $mg \cdot L^{-1}$ BB + 10 $mg \cdot L^{-1}$ TU and for 50 $mg \cdot L^{-1}$ CP + 10 $mg \cdot L^{-1}$ TU, respectively. Comparison to N 1s spectra of single BB and individual TU gives evidence that two peaks of N 1s from BB and TU appear at same position of N1s peak observed in Fig. 8b (399.8 eV) and that observed in Fig. 8a (399.5 eV), respectively. Similar observation that two N 1s chemical states are corresponding to the peaks of N 1s from CP (400.3 eV) and TU (399.5 eV), is obtained from the inspection in Fig. 8e. These conclusions corroborate that BB or CP can be adsorbed jointly with TU on the mild steel surface when BB/TU or CP/TU mixture is employed.

The high-resolution XPS spectrum of S 2p and its line deconvolution curve for mild steel immersed in the solution containing 10 $mg \cdot L^{-1}$ TU is illustrated in Fig. 9a. As shown in Fig. 9a, two S 2p peaks are observed, which indicate that S appears in two chemical states. The first component located at around 162.5 eV [42] corresponds to a bond between the thiourea sulfur atom and metal surface. Thiourea can be oxidized in acid solution when heated and the final product is sulfate [43]. Therefore, the second component can be ascribed to the presence of SO_4^{2-}.

Figs. 9b and 9c present the high-resolution XPS spectra at the binding energy range from 160.0 eV to 170.0 eV for individual 100 $mg \cdot L^{-1}$ BB or 50 $mg \cdot L^{-1}$ CP, respectively. No obvious peak signal of S 2p is observed in these spectra, which indicates BB or CP does not have sulfur element or the components containing sulfur in CP are not adsorbed on the surface of mild steel.

The high-resolution XPS spectra of S 2p and their line deconvolution curves for mild steel immersed in the solution containing 100 $mg \cdot L^{-1}$ BB + 10 $mg \cdot L^{-1}$ TU and 50 $mg \cdot L^{-1}$ CP + 10 $mg \cdot L^{-1}$ TU are shown in Figs. 9d and 9e, respectively. Similarly, two components are necessary to fit the spectra like Fig. 9a and the components are same with TU on account of the absence of S 2p peak in spectra for the situation when BB or CP is used alone. This suggests thiourea in inhibitor blends is adsorbed on the surface of steel when the mixture of BB/TU or CP/TU is added in the corroding solution.

Based on the obtained result, it can be made a conclusion that BB or CP, jointly with TU, is adsorbed on the metal surface.

3.4 Adsorption isotherm

It is well known that the corrosion processes is retarded by the adsorption of corrosion inhibitors on the metal surface. The coverage (θ) of corrosion inhibitor on the surface of metal, which is calculated as $\theta=\eta/100$ [44], is usually used as parameter for the investigation of the adsorption behavior of the inhibitor. The surface coverage value of different concentrations of inhibitor mixtures were obtained from EIS data and are used for calculation with the most appropriate adsorption isotherm. The best fit was obtained with Langmuir isotherm [45] after evaluating several other adsorption isotherms such as Temkin [46, 47], Frumkin [48], and Freundlich [49] isotherms. The Langmuir adsorption isotherm can be expressed as follow:

$$\frac{\theta}{\theta\text{-}1} = K_{ads}C \qquad (4)$$

and rearranging it gives:

$$\frac{C}{\theta} = \frac{1}{K_{ads}} + C \qquad (5)$$

where K_{ads} is the equilibrium constant of the adsorption-desorption reaction, C is the inhibitor (BB or CP) concentration in inhibitor mixture.

Fig. 10 illustrates the Langmuir adsorption plot for mild steel in CO2 saturated solution containing different concentrations of inhibitor mixtures.

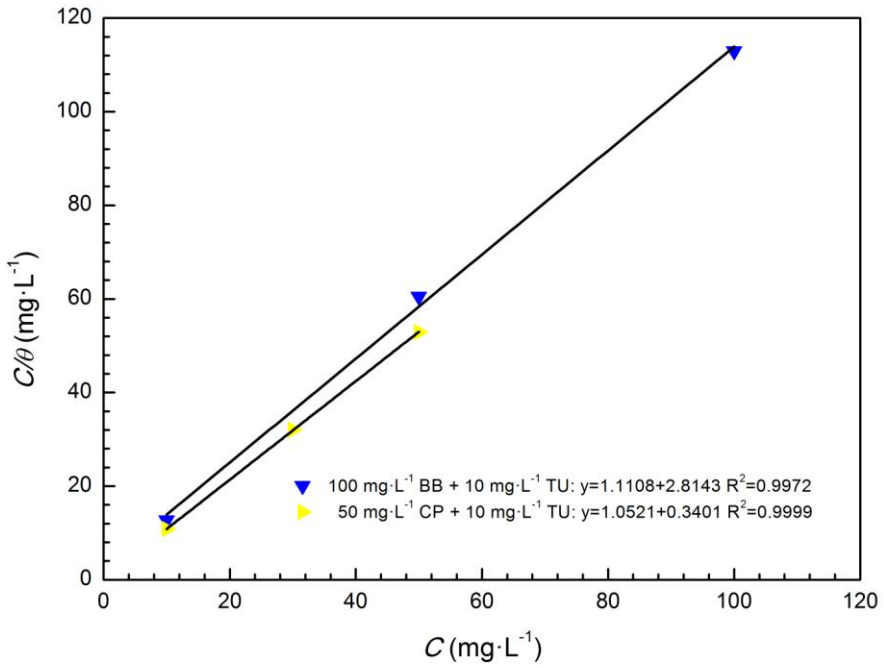

Figure 10. The relationship between C/θ and C in CO_2 saturated 3% NaCl solution in the presence of 10 mg·L^{-1} TU and different concentrations of BB or CP at 60 ˚C (EIS measurement, immersion time is 24 h).

As shown in Fig. 10, plotting C/θ against C gives straight line close to unit slope, suggesting that the adsorption of inhibitor mixtures on the surface of mild steel follows the Langmuir adsorption isotherm [50, 51].

The adsorption of organic inhibitor molecules from the aqueous solution can be regarded as a substitution of the adsorption process between the organic compound in the aqueous phase [$Org_{(sol)}$] and the water molecules adsorbed on the surface of steel electrode as follow [52]:

$$Org_{(sol)} + xH_2O_{(ads)} \leftrightarrow Org_{(ads)} + xH_2O_{(sol)} \quad (6)$$

where x is number of water molecules replaced by the adsorbed molecules.

K_{ads} is related to the standard free energy of adsorption (ΔG_{ads}) according to the following equation [53]:

$$K_{ads} = \frac{1}{1\times10^6}\exp\left(\frac{-\Delta G_{ads}}{RT}\right) \quad (7)$$

where R is universal gas constant, 8.3144 $J\cdot K^{-1}mol^{-1}$, T is the absolute temperature in K. The value of 1×10^6 is the concentration of water in solution expressed in milligram per litre [54].

It was mentioned in some literatures that the values of ΔG_{ads} up to -20 $kJ\cdot mol^{-1}$ are assigned for electrostatic interaction between charged molecules and a charged metal (physisorption), and ΔG_{ads} values around or more negative than -40 $kJ\cdot mol^{-1}$ involve charge sharing or transfer from the inhibitor molecules to the metal surface to form a coordinate type of bond (chemisorption) [19, 44, 49].

When 100 $mg\cdot L^{-1}$ BB + 10 $mg\cdot L^{-1}$ TU is employed, the value of ΔG_{ads} is found to be -35.38 $kJ\cdot mol^{-1}$, and the value of ΔG_{ads} turns out to be -41.24 $kJ\cdot mol^{-1}$ when 50 $mg\cdot L^{-1}$ CP + 10 $mg\cdot L^{-1}$ TU is added into the corroding solution. The ΔG_{ads} value for 100 $mg\cdot L^{-1}$ BB + 10 $mg\cdot L^{-1}$ TU is between -20 $kJ\cdot mol^{-1}$ and -40 $kJ\cdot mol^{-1}$, which suggests that the adsorption mechanism on steel surface might be due to both physisorption and chemisorption, and the adsorption form for 50 $mg\cdot L^{-1}$ CP + 10 $mg\cdot L^{-1}$ TU, which ΔG_{ads} value is lower than -40 $kJ\cdot mol^{-1}$, can be assigned to chemisorptions. The negative values of ΔG_{ads} indicate the adsorption of inhibitor mixtures onto mild steel surface is spontaneous. Compared with BB/TU mixture, the combined use of CP and TU has a more negative ΔG_{ads} value, suggesting that their adsorption is more stable and desorption is more difficult to take place. That is to say, the protection effect of CP/TU is better than BB/TU.

3.5 Synergistic inhibition effect of BB and CP with TU

The synergism parameter (s) is commonly used to further determine whether synergistic inhibition effect is occurrence [55] and defined as follow:

$$s = \frac{1-\theta_A-\theta_B+\theta_A\theta_B}{1-\theta_{AB}} \quad (8)$$

where θ_A and θ_B are the surface coverage of compound A, respectively, B, acting alone, and θ_{AB} is that of the mixture.

The expression actually compares the theoretically expected corrosion rate (numerator), based on the known rates when either compound A or B is present and on the condition that they do not

interact, with the experimentally observed rate in the presence of the inhibitor mixture (denominator) [56].

When no interaction between the two inhibition compounds exists, the value of *s* is equal to unity. Otherwise, the $s > 1$ and $s < 1$ correspond to synergistic effect and antagonistic effect, respectively [57].

The values of *s* for different concentrations of BB or CP with 10 $mg \cdot L^{-1}$ TU are listed in Table 3.

Table 3. Values of the synergism parameter (*s*) for different concentrations of BB or CP with 10 $mg \cdot L^{-1}$ TU.

Inhibitor concentration ($mg \cdot L^{-1}$)			Synergism parameter		
BB	CP	TU	θ_A	θ_B	*s*
10	0	10	0.0176	0.7364	1.169
50	0	10	0.8201	0.7364	1.361
100	0	10	0.8814	0.7364	1.871
0	10	10	0.9220	0.7364	3.049
0	30	10	0.9352	0.7364	3.483
0	50	10	0.9432	0.7364	3.172

As shown in Table 3, all of the *s* values are above 1, which prove that a true synergistic corrosion inhibition effect is present when BB/TU or CP/TU mixture is accessed, no matter how much the adoptive concentration is. The growing *s* value with inhibitor concentration indicates that the synergism becomes stronger when BB or CP concentration in corresponding inhibitor mixture increases. At each concentration, *s* follows the order: CP/TU > BB/TU, suggesting that the synergistic effect for coptis extract is stronger than that for its major component [58].

4. CONCLUSIONS

(1) Coptis extract and its major component berberine are moderate inhibitors for the corrosion of L360 mild steel in CO_2 saturated 3% NaCl solution. The inhibition performance is ordinary and can be improved with the presence of thiourea.

(2) Individual BB or CP acts as mixed-type inhibitor, while the mixture of BB/TU or CP/TU behaves as cathodic inhibitor since E_{corr} shifts to anodic direction.

(3) The inductive loop in the Nyquist plot disappears when single TU or the mixtures is employed compared to the use of individual BB or CP, indicating that corrosion process is completely under charge transfer control.

(4) The lower i_{corr} value and higher R_t value of inhibitor mixtures compared with individual BB, CP or TU suggest that the inhibition effect of inhibitor mixtures are better than that of each inhibitor. These results prove the synergistic corrosion inhibition effect is presence between BB/CP and TU. In

both potentiodynamic polarization method and electrochemical impedance spectroscopy measurement, the inhibition efficiency increases with the increase in inhibitor concentration, no matter for individual use or the mixtures.

(5) The adsorption of BB/TU or CP/TU obeys Langmuir adsorption isotherm. The more negative ΔG_{ads} value for CP/TU compared to BB/TU confirms the adsorption ability of coptis extract is stronger than that of its major component when each of them is combined use with 10 $mg \cdot L^{-1}$ TU.

(6) All the synergism parameters calculated from the applications with different inhibitor concentrations are higher than unity, which confirms there is a true synergistic inhibition effect existing in the BB/TU or CP/TU blends in the research system.

ACKNOWLEDGEMENT
The authors are grateful to the National Natural Science Foundation of China (51471021) for support of this work.

Reference

1. C.B. Pradeep Kumar and K.N. Mohana, *Egypt. J. Petrol.*, 23 (2014) 201
2. H. Ashassi-Sorkhabi, D. Seifzadeh and M.G. Hosseini, *Corros. Sci.*, 50 (2008) 3363
3. S.A. Ali, M.T. Saeed and S.U. Rahman , *Corros. Sci.*, 45 (2003) 253
4. A.K. Satapathy, G. Gunasekaran, S.C. Sahoo, K. Amit and P.V. Rodrigues, *Corros. Sci.*, 51 (2009) 2848
5. A. Ostovari, S.M. Hoseinieh, M. Peikari, S.R. Shadizadeh and S.J. Hashemi, *Corros. Sci.*, 51 (2009) 1935
6. Y. Li, P. Zhao, Q. Liang and B.R. Hou, *Appl. Surf. Sci.*, 252 (2005) 1245
7. A. Bouyanzer, B. Hammouti and L. Majidi, *Mater. Lett.*, 60 (2006) 2840
8. A.Y. El-Etre, *Appl. Surf. Sci.*, 252 (2006) 8521
9. P.C. Okafor, M.E. Ikpi, I.E. Uwah, E.E. Ebenso, U.J. Ekpe and S.A. Umoren, *Corros. Sci.*, 50 (2008) 2310
10. A.M. Abdel-Gaber, B.A. Abd-El-Nabey and M. Saadawy, *Corros. Sci.*, 51 (2009) 1038
11. T. Ibrahim, H. Alayan and Y.A. Mowaqet, *Prog. Org. Coat.*, 75 (2012) 456
12. D. Prabhu and P. Rao, *J. Environ. Chem. Eng.*, 1 (2013) 676
13. S. Garai, S. Garai, P. Jaisankar, J.K. Singh and A. Elango, *Corros. Sci.*, 60 (2012) 193
14. J.S. Choi, J.H. Kim, M.Y. Ali, B.S. Min, G.D. Kim and H.A. Jung, *Fitoterapia*, 98 (2014) 199
15. J.H. Chen, H.Q. Zhao, X.R. Wang, F.S. Lee, H.H. Yang and L. Zheng, *Electrophoresis*, 29 (2008) 2135
16. H.A. Jung, N.Y. Yoon, H.J. Bae, B.S. Min and J.S. Choi, *Arch. Pharm. Res.*, 31 (2008) 1405
17. J. Sun, J.S. Ma, J. Jin, H.S. Wang, Q.H. Wen, H.G. Zhang and Q.L. Zhou, *Acta Pharm. Sin.*, 41 (2006) 380
18. A. Singh, Y.H. Lin, W.Y. Liu, S.J. Yu, J. Pan, C.Q. Ren and K.H. Deng, *J. Ind. Eng. Chem.*, 20 (2014) 4276
19. P.C. Okafor, C.B. Liu, X. Liu, Y.G. Zheng, F. Wang, C.Y. Liu, F. Wang, *J. Solid State Electr.*, 14 (2010) 1367
20. A.C. Makrides and N. Hackerman, *Ind. Eng. Chem.*, 47 (1955) 1773
21. K.C. Pillai and R. Narayan, *J. Electrochem. Soc.*, 125 (1978) 1393
22. B.G. Ateya, B.E. El-Anadouli and F.M. El-Nizamy, *Corros. Sci.*, 24 (1984) 497
23. S. Mendez, G. Andreasen, P. Schilardi, M. Figueroa, L. Vázquez, R.C. Salvarezza and A.J. Arvia,

Langmuir, 14 (1998) 2515
24. M.K. Awad, *J. Electroanal. Chem.*, 567 (2004) 219-225.
25. M.J. Bonné, M. Helton, K. Edler and F. Marken, *Electrochem. Commun.*, 9 (2007) 42
26. J. Zhao, N. Li, S. Gao and G.F. Cui, *Electrochem. Commun.*, 9 (2007) 2261-2265.
27. J.M. Zhao and G.H. Chen, *Electrochim. Acta*, 69 (2012) 247
28. L. Kouisni, M. Azzi, M. Zertoubi, F. Dalard and S. Maximovitch, *Surf. Coat. Technol.*, 185 (2004) 58
29. S.D. Zhu, A.Q. Fu, J. Miao, Z.F. Yin, G.S. Zhou and J.F. Wei, *Corros. Sci.*, 53 (2011) 3156
30. A. Popova, M. Christov, S. Raicheva and E. Sokolova, *Corros. Sci.*, 46 (2004) 1333
31. J. Wang, C.N. Cao, J.J. Chen, M.D. Zhang, G.D. Ye and H.C. Lin, *J. Chin. Soc. Corros. Prot.*, 15 (1995) 241
32. Q. Qu, Z.Z. Hao, L. Li, W. Bai, Y.J. Liu and Z.T. Ding, *Corros. Sci.*, 51 (2009) 569
33. M.A. Veloz and I.González, *Electrochim. Acta*, 48 (2002) 135
34. P.C. Okafor, C.B. Liu, X. Liu and Y.G. Zheng, *J. Appl. Electrochem.*, 39 (2009) 2535
35. K.W. Tan, M.J. Kassim and C.W. Oo, *Corros. Sci.*, 65 (2012) 152
36. M.A. Amin, S.S.A. El-Rehim, E.E.F. El-Sherbini and R.S. Bayoumi, *Electrochim. Acta*, 52 (2007) 3588
37. K. Jüttner, *Electrochim. Acta*, 35 (1990) 1501
38. T. Pajkossy, *J. Electroanal. Chem.*, 364 (1994) 111
39. H.Y. Ma, X.L. Cheng, G.Q. Li, S.H. Chen, Z.L. Quan, S.Y. Zhao and L. Niu, *Corros. Sci.*, 42 (2000) 1669
40. A.V. Benedeti, P.T.A. Sumodjo, K. Nobe, P.L. Cabot and W.G. Proud, *Electrochim. Acta*, 40 (1995) 2657
41. M.V. Azghandi, A. Davoodi, G.A. Farzi and A. Kosari, *Corros. Sci.*, 64 (2012) 44
42. M. Quinet, F. Lallemand, L. Ricq, J.Y. Hihn and P. Delobelle, *Surf. Coat. Tech.*, 204 (2010) 3108
43. Q.F. Zeng, F. Yu, G.N Dong and J.H. Mao, *Appl. Surf. Sci.*, 259 (2012) 83
44. X.Y. Zhang, F.P. Wang, Y.F. He and Y.L. Du, *Corros. Sci.*, 43 (2001) 1417
45. E.A. Noor and A.H. Al-Moubaraki, *Mater. Chem. Phys.*, 110 (2008) 145
46. P.C. Okafor, X. Liu and Y.G. Zheng, *Corros. Sci.*, 51 (2009) 761
47. P.C. Okafor and Y.G. Zheng, *Corros. Sci.*, 51 (2009) 850
48. E.E. Oguzie, Y. Li and F.H. Wang, *J. Colloid Interf. Sci.*, 310 (2007) 90
49. I.B. Obot and N.O. Obi-Egbedi, *E-J. Chem.*, 7 (2010) 837
50. G.N. Mu, X.H. Li, Q. Qu and J. Zhou, *Corros. Sci.*, 48 (2006) 445
51. M.A. Hegazy, M. Abdallah and H. Ahmed, *Corros. Sci.*, 52 (2010) 2897
52. [S.K. Shukla and M.A. Quraishi, *Corros. Sci.*, 51 (2009) 1007
53. R. Fuchs-Godec and V. Doleček, *Colloid. Surface A*, 244 (2004) 73
54. X.H. Li, S.D. Deng and H. Fu, *Corros. Sci.*, 62 (2012) 163
55. T. Murakawa, S. Nagaura and N. Hackerman, *Corros. Sci.*, 7 (1967) 79
56. U.M. Eduok, S.A. Umoren and A.P. Udoh, *Arab. J. Chem.*, 5 (2012) 325
57. S.A. Umoren, O. Ogbobe, I.O. Igwe and E.E. Ebenso, *Corros. Sci.*, 50 (2008) 1998
58. X.H. Li, S.D. Deng, H. Fu and X.G. Xie, *Corros. Sci.*, 78 (2014) 29